Inductive sustainment of oblate field-reversed configurations with the assistance of magnetic diffusion, shaping, and finite-Larmor radius stabilization

S. P. Gerhardt,[1] E. V. Belova,[1] M. Yamada,[1] H. Ji,[1] M. Inomoto,[2] C. M. Jacobson,[1] R. Maqueda,[3] B. McGeehan,[1] and Y. Ren[1,a)]
[1]*Princeton Plasma Physics Laboratory, Princeton, New Jersey 08543, USA*
[2]*Osaka University, Osaka 565–0871, Japan*
[3]*Nova Photonics, Princeton, New Jersey 08540, USA*

(Received 24 September 2007; accepted 3 January 2008; published online 15 February 2008)

Oblate field-reversed configurations (FRCs) have been sustained for >300 μs, or >15 magnetic diffusion times, through the use of an inductive solenoid. These argon FRCs can have their poloidal flux sustained or increased, depending on the timing and strength of the induction. An inward pinch is observed during sustainment, leading to a peaking of the pressure profile and maintenance of the FRC equilibrium. The good stability observed in argon (and krypton) does not transfer to lighter gases, which develop terminal co-interchange instabilities. The stability in argon and krypton is attributed to a combination of external field shaping, magnetic diffusion, and finite-Larmor radius effects. © *2008 American Institute of Physics*. [DOI: 10.1063/1.2837512]

I. INTRODUCTION

The field-reversed configuration (FRC)[1] is unique among the class of toroidal magnetically confined plasmas, in that the plasma is not linked by toroidal coils, possesses a natural divertor, and has $\beta \sim 1$ (β is the ratio of kinetic pressure to magnetic pressure, defined here as $\beta = 2\mu_0 \langle P \rangle / \langle B^2 \rangle$, where $\langle \ldots \rangle$ represents an average over the plasma volume). These unique features have led to interest in the FRC as the core of a fusion power plant.[2] For instance, the absence of toroidal field coils allows the plasma to be translated[3,4] away from the formation region and into a burn region, so that these two chambers can have different designs. The high-β provides for a compact reactor core, and allows the prospect of using advanced fuels.[2] These unique features have also led to interest in the FRC as a fueling source for other large magnetized plasmas,[5,6] and as test-beds for the basic studies of high-β magnetized plasmas.[4,7] However, there are a host of physics issues that must be resolved in order for the FRC to fully realize its potential.

One issue is related to the sustainment of the configuration for many current diffusion times. Historically, most FRCs have been allowed to resistively decay after formation. More recently, techniques have been proposed and/or utilized to sustain the plasma, including neutral beam injection (NBI)[8,9] and rotating magnetic fields (RMF)[10–26] in axially elongated prolate FRCs. For the more spherical oblate FRC, inductive sustainment[27–29] has been utilized with some success. The continued development of FRC sustainment schemes would help both the reactor prospects and the basic understanding of these configurations.

A second issue of great importance is the stability of these configurations. The everywhere bad curvature of the FRC has led to the prediction that these plasmas should be violently unstable[30–43] to pressure driven instabilities known as co-interchange modes, a category that includes the famous tilt-instability.[31,32] The predicted instability growth times are approximately equal to the time required for an Alfven wave to traverse the system. However, most FRCs have been experimentally stable to these instabilities, often lasting many Alfven times as they decay.[44] The cause of this apparent stability has most often been attributed to finite-Larmor radius (FLR) stabilization.[45] The exception to the observation of co-interchange stability comes from the oblate FRC, where these modes have been observed and their behavior studied as a function of plasma shape,[46] with and without passive stabilizers. It has been predicted that FLR stabilization will be more difficult in oblate FRCs[39] than their prolate cousins, but that stabilization by a beam of high-energy ions could lead to a macroscopically stable oblate FRC.[43,47] Hence, the experimental extension of FLR studies to the oblate regime is an important step.

While these topics of stability and sustainment may at first appear to be separate, they are actually tightly coupled. On the one hand, an unstable plasma cannot be sustained. On the other hand, sustainment is necessary to test the long-time stability of these configurations. In this paper, we report coupled stability and sustainment results for oblate FRCs produced in the Magnetic Reconnection Experiment (MRX).[48]

Sustainment of an oblate FRC has been demonstrated in MRX utilizing solenoid induction. Argon plasmas have been sustained for >300 μs, corresponding to >15 poloidal flux confinement times in some cases. The poloidal flux can be sustained or increased, depending on the choice of induction timing and voltage, and the sustainment process has been understood as a balance between an inward pinch and outward diffusion. Initial transport analysis has been completed, showing that the diffusion of particles and poloidal flux are consistent with classical predictions, i.e., outward diffusion

a)Present address: Department of Physics, University of Wisconsin–Madison, Madison, WI 53706, USA.

 © 2008 American Institute of Physics

Downloaded 21 Jul 2008 to 198.35.13.204. Redistribution subject to AIP license or copyright; see http://pop.aip.org/pop/copyright.jsp

rate proportional to the pressure gradient and the collisional resistivity.

These argon FRCs do not show any sign of performance-limiting instabilities. The observed good stability, however, is not observed to transfer to FRCs formed from lighter gases. Deuterium and helium plasmas often succumb to instabilities even before the solenoid current ramp begins, and cannot be sustained. Nitrogen and neon plasmas typically show some period of sustainment, but are ultimately terminated short of the longest possible lifetime. The observed magnetic perturbations grow on the Alfven transit-time, and have the features expected from the co-interchange instability. A stability analysis indicates that at least three effects play a role in stabilizing the long-lived argon plasmas. Proper shaping of the equilibrium field during the sustained period, in that $n_{\mathrm{decay}} \approx -R/B_Z \partial B_Z/\partial R > 1$, contributes to $n=1$ (tilt) stability for plasmas that survive into that portion of the discharge. The low electron temperature (generally $T_e = 6-9$ eV) in these plasmas leads to a rather large electrical resistivity, which can help to damp out instabilities. Finally, finite-Larmor radius effects contribute to the stability of $n=3$ and 4 modes in argon plasmas.

The remainder of this paper is organized as follows. Section II describes relevant previous studies of FRC sustainment and stability, while Sec. III describes the MRX facility as configured for sustained FRC studies. Section IV provides examples of the evolution of typical sustained FRCs, and Sec. V describes systematic studies of FRC under sustainment. The discussion of FRC stability is given in Sec. VI, while conclusions are given in Sec. VII.

II. PREVIOUS STUDIES OF FRC SUSTAINMENT AND STABILITY

There are a number of proposed schemes for the sustainment of FRC configurations, some of which have been tested in experiments. The first part of this section provides an overview of some of these sustainment schemes, including rotating magnetic fields (RMF), neutral beam current drive, and inductive sustainment. A brief review of co-interchange stability is then provided, including a discussion of possible stabilizing effects. No claim is made to be comprehensive in either discussion.

A. FRC sustainment

RMF current drive[10,23] is the most heavily studied and successful method for sustaining a prolate FRC (prolate FRCs have elongation $E = Z_S/R_S > 1$, where Z_S and R_S are the maximum axial and radial locations on the separatrix). This technique was developed in a series of rotomak experiments at Flinders University,[12] and has subsequently been applied to the prolate FRC with good success. A first experiment in STX (Star Thrust Experiment) was able to generate axial field reversal significantly larger than the magnitude of the rotating field,[14] and to maintain the field-reversed configuration for as long as the RMF was applied, and subsequent experiments have expanded the operational regime and physics basis of this technique. It has been applied both to sustain a plasma formed by theta-pinch initiation[14] and to form an FRC from a uniform axial field with a pre-ionized fill;[17,20] it has sustained the configuration when the antennas were located outside of an insulating vacuum chamber,[23] or inside an all-metal chamber.[22]

RMF applies a rotating transverse magnetic field to the plasma, leading to a time-dependent axial electric field. The in-phase oscillation between the driven electron current and the radial magnetic field (from the RMF) produces an azimuthal force on the electrons $F_{\phi,\mathrm{RMF}} = -n_e e \langle v_{ez} B_R \rangle$ over the region where the RMF penetrates. The penetration depth of the RMF (δ), however, is not set by the classical electromagnetic skin depth, but is instead given by $\delta^* = [2\eta/\mu_0(\omega - \omega_e)]^{1/2}$, where ω is the RMF frequency, and ω_e is the electron rotation frequency. The penetration is enhanced compared with the classical value, because in the frame of the electron rotation, the RMF frequency appears to be much lower.[14] Given this penetration depth and form for the azimuthal force, it is possible to calculate the torque on the electrons per antenna length as $T_{\mathrm{RMF}} = 2\pi r_s \delta^* B_\omega^2/\mu_0$,[13] where r_s is the separatrix radius and B_ω is the RMF field. The azimuthal current and poloidal flux will increase until the RMF torque on the electrons is balanced by the resistive torque $T_\eta = \frac{1}{2}\pi e^2 \langle n_e^2 \omega_e \eta \rangle r_s^4 l_s$ with $l_s = 2Z_s$ the separatrix length and η is the plasma resistivity. Equating these torques indicates the steady-state density possible for a given RMF field, frequency, and plasma resistivity, which then scales as $B_\omega/\omega^{1/2}$. Good agreement with this scaling was found in RMF experiments in the TCS (Translation, Confinement, and Sustainment) experiment.[17] Using a rigid-rotor equilibrium to analyze the measurements, it was found that the resistivity was enhanced beyond that of a typical FRC when the RMF field magnitude exceeded a threshold of ~30% of the external field.[17]

Simulations have been used to better understand the method of driving currents throughout the FRC volume. A study by Milroy[15] demonstrated the means by which Ohm's law is satisfied, so that $E_\phi^0 = V_R^0 B_Z^0 + \eta J + \langle J_Z^1 B_R^1 \rangle / en = 0$ throughout the FRC volume during the sustainment phase. The simulations indicated that the $\langle J_Z^1 B_R^1 \rangle / en$ RMF drive extended to just beyond the field null, so that this term could balance the electric field at the null. A large radially inward flow was observed, which provided a $V_R^0 B_Z^0$ term to balance the ηJ term inside the null and weaken the $\langle J_Z^1 B_R^1 \rangle / en$ term outside the null, allowing $E_\phi^0 = 0$ everywhere. This inward flow then followed the field lines around the ends of the FRC and back to the outboard side, thus satisfying continuity. It is this radial flow that redistributed the RMF torque throughout the FRC in the torque balance described above.[13,14]

More recent studies have observed that the resistivity profiles in these RMF driven FRCs can be highly nonuniform, with edge resistivities 100 (or more) times the core resistivity.[20] In these cases, the RMF was not observed to penetrate to the field null; this made sustainment difficult to understand in the context of the discussion in the previous paragraph. Simulations with highly nonuniform resistivity were performed that showed a two-layer structure, with the core plasma rotating more slowly than the edge; the differential rotation led to a tearing and reconnection process,

Downloaded 21 Jul 2008 to 198.35.13.204. Redistribution subject to AIP license or copyright; see http://pop.aip.org/pop/copyright.jsp

which transferred torque to the inner region.[18] The fluctuation signature of this reconnection process was observed in both simulation and experiment. A regime of improved confinement with a spheromak-like plasma core was identified in some of these plasmas, and was interpreted as a sign of non-Taylor relaxation.[24]

One concern with RMF has been with regard to the opening of magnetic field lines (all magnetic field lines are of course ultimately closed; open in this context means that they would close outside the walls of the confinement chamber); for sufficiently slow magnetic diffusion, parallel transport can remove heat and particles on the open field lines. Calculations showed that the flux surfaces undergo a shift and tilt when a transverse field is applied;[11] further research showed that the magnetic field lines do indeed become open, even for very small RMF field magnitude.[49] The method of odd-parity RMF, where the transverse field has odd symmetry about the midplane, was suggested as a means of maintaining field-line closure,[16] and stochastic ion heating by odd-parity RMF has been demonstrated in simulation.[25] Recent results from TCS have found a dramatic improvement in FRC confinement with odd-parity RMF compared to the standard even-parity case.[21] The Princeton FRC, using odd-parity RMF, showed the production of high-T_e plasmas at very low Coulomb collisionality, with full RMF penetration to the major axis of the device.[26]

While the odd-parity scheme has proven effective and now appears to be the preferred approach to RMF in an FRC, the success of these techniques does not obviate the need for other sustainment research via other techniques. For instance, supplementing RMF with core current drive would be an attractive feature. Also, the detailed scaling of the technique to hotter plasmas has not been demonstrated [though recent results from TCS upgrade (TCSU)[50] are very encouraging in this regard], and the transport consequences of field line opening, of larger concern with even-parity RMF, but also possible with imperfect odd-parity RMF, have not been fully evaluated.

A second sustainment technique that has received attention is neutral beam injection (NBI). This has been proposed in a prominent FRC reactor study,[2] and in the context of driving current at the FRC null[20] during RMF sustainment. A detailed study of tangential neutral beam current drive in a prolate FRC, using a self-consistent equilibrium, was reported in Lifschitz *et al.*[8] For large beam currents, a distortion of the plasma equilibrium leading to a midplane peaking of the beam current density was reported. The beam driven current and its spatial distribution were only weakly modified by the injection impact parameter. The dependence of the beam driven current on the injected neutral beam current deviated from linearity, due to effects such as the increase in density at the midplane and the self-focusing of the beam in that high-density central region. A further study addressed the current drive efficiency for the likely parameters of next-generation RMF driven FRCs.[9] Injection into the ends of the FRC led to low power deposition and low current drive efficiency, due to rapid loss of particles to the vacuum vessel wall. Good current drive efficiency was possible for tangential injection, with little dependence on the axial location of injection as long as it was within the FRC itself. Importantly, tangential NBI was found to be compatible with RMF, provided that the RMF magnitude was $<5\%$ of the axial field and that it did not penetrate beyond $0.1R_S$. Note that other studies have examined the injection of a neutral beam for the stabilization of the tilt instability[51] or the higher-n co-interchange modes.[43]

Neutral beam injection into an FRC has been tested in the FIX (FRC Injection Experiment) device.[52] As indicated above, NBI can only drive current if the magnetic field is sufficiently strong to contain the energetic ion orbits. This problem was resolved in the FIX experiments by injecting at 19.3° with respect to the geometric axis of the device, so that the particles would be trapped in the magnetic mirrors at the FRC ends. The separatrix volume decay rate was reduced when NBI was used. The improvement in the energy confinement time was greatest when high magnetic mirror ratios were used, even though these high mirror ratio configurations showed a degradation in confinement without NBI.[53] The injection was not, however, optimized for current drive and no beam-driven currents were reported. The cause of the confinement improvement with NBI was not clear, and it was hypothesized that the large-orbit ions might create potential barriers that improve the thermal confinement. The NBI was also observed to assist in the stabilization of FRC global motion.[54]

Two other sustainment techniques have received theoretical attention, though without experimental study. Thermoelectric sustainment is based on the observation that more energetic electrons collide less efficiently than cold ones (as v_r^{-3}, where v_r is the relative velocity). This can give rise to a net force that cancels the normal friction force, and thus may allow for a steady-state FRC provided that the electron temperature gradient can be maintained.[55] For a thermonuclear FRC, studies have shown that some charged fusion products directly escape the configuration, while others are confined to form a flow in the same direction as the equilibrium plasma current. This flow can generate a current as large as the original field-reversing current, and can be used to sustain the configuration.[56]

The above noted sustainment schemes have usually been examined in the context of the axially elongated prolate FRC. However, there are technical reasons to expect that a more oblate shape may be advantageous for FRC performance. From the magnetohydrodynamic (MHD) stability standpoint, the tilt instability becomes an external mode when the elongation, E, becomes less than 1.[35,39] Simulations show that this external tilt can be stabilized with nearby passive stabilizers,[39] and experimental results confirm this.[46] From a transport perspective, the oblate shape maximizes the shortest distance between the hot plasma core and the cooler edge; for diffusive transport, this geometry maximizes the confinement times.[57] From a formation standpoint, the technique of spheromak merging has been utilized to form large-flux oblate FRCs.[44,58,59]

In principle, many of the sustainment techniques noted above are applicable to the oblate FRC. Indeed, sustainment by NBI has been proposed as part of the SPIRIT oblate FRC program.[47] However, the oblate shape allows for an addi-

Downloaded 21 Jul 2008 to 198.35.13.204. Redistribution subject to AIP license or copyright; see http://pop.aip.org/pop/copyright.jsp

tional sustainment technique: inductive sustainment via a solenoid. Inductive sustainment of an FRC was first demonstrated in the TS-3 spheromak merging device, where a preliminary experiment demonstrated sustainment of small (trapped poloidal flux $\psi_t < 0.7$ mWb) FRCs for ~ 200 μs.[27] These experiments were continued in the larger TS-4 device,[28] where sustainment of a larger flux FRC ($\psi_t \approx 3$ mWb) was demonstrated for >250 μs in argon discharges. These experiments provided important evidence that FRC sustainment via inductive current drive was possible. The present work expands on those results by extending the period of sustainment, by estimating transport properties, and by exploring the stability of sustained FRCs formed in different gases. This work was briefly summarized in Ref. 29. Note that repetitive spheromak merging has also been suggested as a means to sustain an oblate FRC.[58]

B. Stability of FRC configurations

A second area of intense FRC research focuses on macroscopic stability. Generically speaking, the magnetic field curvature in an FRC points opposite the pressure gradient at all points in the plasma. This configuration, known as having "bad curvature," is unstable to pressure-driven instabilities called "ballooning" modes in the context of most fusion systems,[60] or "co-interchange" modes in the case of the FRC. These modes result in a bulging outward of the plasma in the region of bad magnetic curvature, and are often more unstable[36] than modes with uniform displacement along the field line (the "interchange" mode[61]).

The co-interchange instability can be divided into axially polarized modes, where the dominant plasma displacement is in the axial direction, and radially polarized modes, where the dominant plasma displacement is radial; the polarization that grows more quickly is determined by factors such as plasma shape.[39] For each of these polarizations, many toroidal mode-numbers are simultaneously unstable. The n=1 axially polarized co-interchange mode is more commonly known as the "tilt" instability,[31,32] while the $n=1$ radially polarized mode is known as the "radial shift" mode. These modes are predicted to have a growth time comparable to the Alfven time,[33,38,40] and have been predicted to terminate the plasma configuration.[35,38,39] Further discussion regarding the co-interchange mode can be found in Ref. 46 and references therein.

Given the theoretical attention paid to these instabilities, it is perhaps surprising that they are not generally considered a problem in present-day prolate FRCs. Results from FRX-C showed evidence of the tilt instability from magnetic signatures measured at the vacuum vessel walls,[62] and these modes were correlated with an enhanced poloidal flux loss rate.[63] Measurements in LSX, however, were unable to detect any sign of the tilt.[64,65] Furthermore, decaying prolate FRCs are often able to last for many Alfven transit times.[44] These prolate FRCs are typically very kinetic (i.e., the ions have Larmor orbits that are comparable to the system size), which should contribute a stabilizing effect. The stability of these modes in a more MHD-like FRC reactor is an open question.

In contrast, these pressure-driven co-interchange modes have indeed been observed in oblate FRCs. The $n=1$ axially polarized co-interchange (the tilt instability) in an oblate FRC is predicted to be an external mode,[35,39] and has been experimentally observed in the Swarthmore Spheromak Experiment (SSX)[59] and MRX.[46] The only observation of the $n=2$ and 3 co-interchange, however, was in oblate FRCs in the MRX device.[46] It was shown there that these modes responded to the effect of external field shaping, and a unique plasma shape was found with improved stability to low-n co-interchange modes. This "negative triangularity" shape was further shown to lead to the nonlinear saturation of the low-n radially polarized modes. These results relied on both flexible plasma shaping and nearby passive conductors to maintain stability for the decaying FRCs. The stability of these configurations under long-time sustainment, and without nearby passive stabilizers or the unique shape, was left as an open question.

Many physics mechanisms outside of simple resistive MHD have been proposed in order to explain the observed stability of prolate FRCs, mostly concentrating on the $n=1$ tilt. These have included toroidal rotation,[34] flow shear,[38] the Hall effect,[66] and finite-Larmor radius (FLR)[38–43,45] stabilization. Calculations have indicated that toroidal velocities on order of the Alfven speed are required for tilt stabilization;[34] this requirement for very high flow speeds holds even in the presence of strong rotation shear.[38] Analytic theory has indicated stabilization from the Hall effect.[66] However, simulations have indicated that the Hall effect significantly modifies the mode eigenfunction,[37,40] but does not lead to stability.

While there is still no consensus, it appears that finite-Larmor radius (FLR) stabilization[45] likely plays a role in the observed stability of prolate FRCs. This effect arises from the different sizes of the Larmor radius of ions and electrons. When an instability grows, there is a perturbed electric field associated with the perturbed currents that drive the instability. In MHD, ions and electrons respond to the electric field in an identical way. When FLR physics are introduced, the average electric field seen by the ions as they execute their large orbits is different from that seen by the electrons, and so differential motion is introduced. These effects create a finite phase shift between the ion-fluid velocity and the mode magnetic field perturbations (to which the electron fluid is tied). This phase shift introduces a reactive effect, which results in a finite real frequency and reduced mode growth rates.[40]

The reactive effect manifests itself by modifying the typical MHD dispersion relationship ($\omega^2 + \gamma_{\mathrm{MHD}}^2 = 0$) to read

$$\omega^2 - \omega^* \omega + \gamma_{\mathrm{MHD}}^2 = 0, \tag{1}$$

where γ_{MHD} is the MHD growth rate and $\omega^* = \mathbf{k} \cdot \mathbf{V}_D$ with $\mathbf{V}_D$ the diamagnetic drift velocity.[66] This expression yields an approximate condition for FLR stabilization to be important for a given mode: $K < 1$, where $K = \gamma_{\mathrm{MHD}} / 2\omega^*$. This condition can be used to derive the more common FRC requirement for FLR to stabilize the tilt: $\bar{s}/E < 0.3$–0.5, where $\bar{s}$ is approximately equal to the volume average number of ion gyroradii between the field null and the outer separatrix and is defined as

Downloaded 21 Jul 2008 to 198.35.13.204. Redistribution subject to AIP license or copyright; see http://pop.aip.org/pop/copyright.jsp

$$\bar{s} = \int_{R_0}^{R_S} \frac{RdR}{R_S \rho_i}. \tag{2}$$

By using $\rho_i = \sqrt{2T_i m_i}/q_i B$ (T_i is a representative average ion temperature, m_i is the ion mass, and q_i is the ion charge) and the definition of the trapped poloidal flux ($\psi_t = 2\pi \int_{R_0}^{R_S} RB_Z dR$), the parameter $\bar{s}$ can be written in terms of typical experimental parameters as[65]

$$\bar{s} = \frac{Z_i \psi_t}{R_S \sqrt{M_i} \sqrt{T_{i,eV}}} \left[\frac{\sqrt{e}}{2^{3/2} \pi \sqrt{m_p}} \right]. \tag{3}$$

The coefficient in square brackets can be evaluated as 1.1×10^3 $\mathrm{eV}^{1/2}$ m^{-1} Wb^{-1}. This parameter $\bar{s}$ will be utilized below for comparison with previous results, though the parameter K will be more useful in the analysis of MRX data.

The role of FLR stabilization has not been totally resolved in theory or experiment. Simulations using both the gyroviscous formulation[40] and with a hybrid code[41] have predicted that FLR effects cannot reduce the tilt mode linear growth rate to zero in a prolate FRC. However, the nonlinear saturation of the tilt instability was observed in hybrid simulations,[42] as the plasma nonlinearly evolved to a new rotating equilibrium from a stationary initial condition. Simulations have also indicated that FLR stabilization is likely to be less effective in an oblate FRC, compared to the prolate case.[39]

Before ending this overview section, it should be noted that although the co-interchange modes are experimentally stable in most prolate FRCs, there is a radially polarized $n=2$ rotational instability that often terminates the discharge.[19,67,68] This instability is driven by the radially outward centrifugal pressure of the rotating FRC. Successful stabilization techniques for this mode involve multipole stabilization[67,68] and RMF.[19]

III. THE MRX DEVICE AND EXPERIMENTAL DESIGN

The experiments reported in this paper were carried out in the Magnetic Reconnection Experiment.[48] This facility was primarily designed to study the basic physics of magnetic reconnection, from both a global and local perspective. One application of magnetic reconnection is the formation of FRCs via spheromak merging, as demonstrated in previous experiments.[69,70,58,59] The results in this paper take this a step further by applying inductive current-drive to the FRC after the spheromak merging is finished. Note that the push-reconnection during the early merging phase has been studied in the context of Hall-reconnection studies.[70] The MRX geometry and hardware configuration for these studies are illustrated in Fig. 1.

Spheromak plasmas are formed in MRX utilizing flux cores;[71] these are doughnut-shaped objects (major radius of 37.5 cm and minor radius of 10 cm) containing both toroidal and helical windings. When the currents in the windings are properly programmed, a spheromak is formed near each flux core. The spheromaks then merge, due to both the attraction of their parallel toroidal currents and the pushing force from toroidal currents in the flux cores. One 360 μF capacitor bank (typical charging voltage of 13 kV) is utilized to power

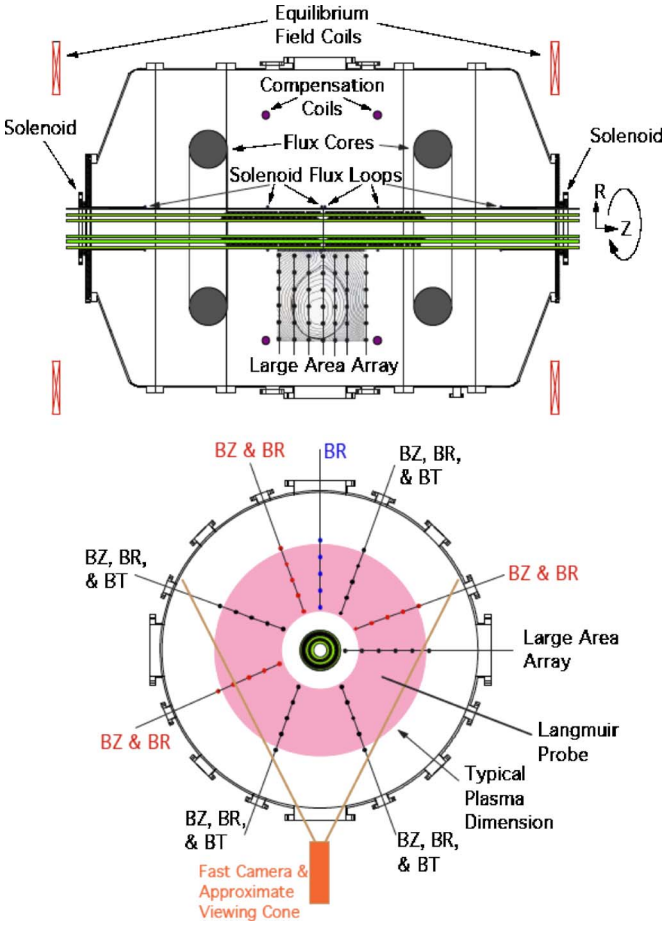

FIG. 1. (Color online) The hardware and diagnostic configuration of MRX for the FRC sustainment experiments.

the toroidal windings in the flux cores, while a 240 μF capacitor bank (typical charging voltage of 14 kV) was used to power the helical winding.

The solenoid system is composed of two separate coils, inserted from the ends of the machine to within ≈3 mm of touching at the midplane. Each of the two solenoid coils contains two 17-turn winding layers ($R=7.5$ cm and 5 cm). Each coil was contained in a separate vacuum jacket, constructed from a 0.13 mm thick Inconel liner along the outer cylinder of the solenoid and a 1.5 mm thick Inconel plate at the midplane end of the coil. This design resulted in a ~2 cm central gap in what would have otherwise been a continuous solenoid winding. This gap, coupled to eddy currents in the Inconel conductors, resulted in some axisymmetric modifications to the plasma shape, as will be apparent below. The two solenoid coils were typically operated in a series connection, and were powered by a 420 μF capacitor bank charged to typically between 6 and 10 kV.

An additional set of two compensation coils was utilized to improve the stability and radial position control. Each compensation coil consisted of two independent single-turn windings inside each coil casing; the radius of the coils was 0.54 m. One winding of each compensation coil was placed in series with the adjacent toroidal windings of the flux core, but with the current oppositely directed compared to that in the flux-core windings. This connection served to push the

Downloaded 21 Jul 2008 to 198.35.13.204. Redistribution subject to AIP license or copyright; see http://pop.aip.org/pop/copyright.jsp

spheromaks away from the midplane during their formation period, and then created moderately good field curvature after merging was completed ($n_{decay} \approx 1/2$; see Sec. VI for details). The second winding of each compensation coil was placed in series with the nearby solenoid. This is because the return flux of the solenoid, which is trapped inside the flux-conserving vacuum vessel, is in the direction to cause a radial expansion of the plasma. The series compensation winding was used to cancel this solenoid return flux (at a single axial and radial location) and thus approximately preserve radial equilibrium. Specially tuned inductors were placed in parallel with each of the four compensation windings, allowing the modifications to the external field from the various sources to be finely tuned.

The primary diagnostics utilized in these studies are two arrays of magnetic probes. One array, known as the Large Area Array, was located at a fixed toroidal angle, and was composed of seven individual linear probe arrays. Each linear array had six coil triplets (B_Z, B_R, and B_T measurements) separated radially by 8 cm. When these data are combined with measurements of the poloidal flux from six loops mounted on the solenoid liner surface ($\psi_{loop}(z)$), it is possible to calculate the poloidal flux as

$$\psi(R,Z;t) = 2\pi \int_{R_{solenoid}}^{R} R' B_Z(R',Z;t) dR' + \psi_{loop}(Z). \quad (4)$$

The trapped poloidal flux is then calculated as $\psi_t = \psi_{sep} - \psi_0$, with ψ_0 the poloidal flux at the field null and ψ_{sep} the poloidal flux at the separatrix [an alternative definition of the trapped flux appears beneath Eq. (2)]. The poloidal flux is then utilized to calculate the toroidal electric field as

$$E_\phi = \frac{1}{2\pi R} \frac{d\psi}{dt}. \quad (5)$$

We also utilize this probe array to calculate the toroidal and poloidal plasma currents as

$$J_T = \frac{1}{\mu_0} \left(\frac{\partial B_Z}{\partial R} - \frac{\partial B_R}{\partial Z} \right), \quad (6)$$

$$\vec{J}_P = \nabla\phi \times \nabla \left(\frac{RB_T}{\mu_0} \right), \quad (7)$$

the plasma pressure from force balance as

$$P(R,Z) = \int_{\psi<\psi_{sep}} (j_R B_T - j_T B_R) dZ, \quad (8)$$

and the toroidal flux as

$$\Phi = \int_{\psi<\psi_{sep}} B_T dA, \quad (9)$$

where the integral in Eq. (9) is over the area enclosed by the separatrix.

The second probe array is composed of eight linear probe arrays located at approximately equally spaced toroidal angles at the midplane, and is called the Spoke Probe Array. Each linear array contains five coil triplets radially separated by 8 cm. The raw signals from the array are decomposed at each time point and radius into sine and cosine components with amplitudes $C_n(R,t)$ and $S_n(R,t)$,

$$B(R,\phi,t) = B_0(R,t) + \sum_{n=1}^{n_{max}} [C_n(R,t)\cos(n\phi) + S_n(R,t)\sin(n\phi)], \quad (10)$$

where B can be any of B_R, B_T, and B_Z. This decomposition allows the study of the time evolution of individual Fourier modes with a time resolution of about 3 μs. Not all coils of the array had their signals digitized; the data collected were sufficient to resolve toroidal mode numbers up to $n=3$ in B_Z and $n=4$ in B_R (the midplane probe of the Large Area Array doubled as a probe in the Spoke Probe Array).

The measured magnetic perturbations were used to identify instabilities via the method described in detail in Ref. 46. The midplane B_R perturbations are interpreted as signs of the axially polarized co-interchange modes, as the poloidal field of the FRC is pulled to the midplane by the axial motion of the plasma. Similarly, the B_Z perturbation can be interpreted in terms of radially polarized co-interchange modes, as the plasma shifting alternatively in and out moves different regions of the axial field gradient onto the fixed radius probes.

In addition to the midplane perturbation information, the poloidal flux can be calculated from the $n=0$ component of B_Z, yielding a truly axisymmetric value. This can in turn be used to calculate the kinetic parameter $\bar{s}$ from Eq. (3), the surface voltage as the time derivative of the separatrix flux, and the total trapped poloidal flux (ψ_t).

IV. SUSTAINMENT EXAMPLES

Representative examples of sustained and unsustained argon FRCs are illustrated in Fig. 2. The poloidal flux contours (0.35 mWb spacing) and toroidal field (colors), as determined by the Large Area Array, are plotted at a sequence of times, for sustained and unsustained discharges. The heavy black line represents the separatrix, while the gray area at the bottom represents the volume of the solenoid. The spheromaks are formed at the flux cores at $t \approx 210$ μs, which were located axially at $Z_{FC} = \pm 0.55$ m for most experiments in this paper, and then begin to approach the midplane. The merging begins at ≈ 280 μs and ends by 295 μs; the residual toroidal fields have been eliminated by 325 μs and an oblate FRC is formed. This FRC remains at the midplane, and the bottom row of the figure indicates that the unsustained configuration resistively decays away by ≈ 360 μs. However, for the case in the upper row, the solenoid is energized at 320 μs. Allowing for the delay caused by the liner currents, there is a loop voltage applied to the plasma from ≈ 340 μs through ≈ 600 μs, with a resulting sustainment of the FRC through this period. Note that the diamond shape acquired by the plasma is due to the combination of solenoid flux leaking through the midplane solenoid gap and the pushing force from the compensation coils.

A similar sequence of events is visible in white-light camera images of the merging and sustainment, as shown in Fig. 3. The camera views nearly the entire plasma in this example, as indicated in Fig. 1. The solenoid is visible as a

Downloaded 21 Jul 2008 to 198.35.13.204. Redistribution subject to AIP license or copyright; see http://pop.aip.org/pop/copyright.jsp

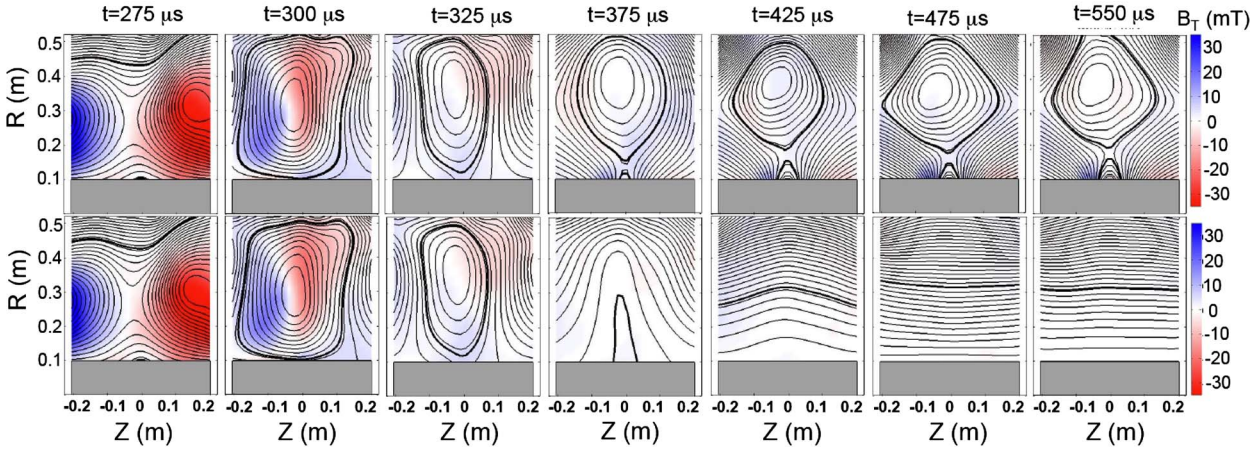

FIG. 2. (Color online) The poloidal flux (contours) and toroidal field (colors) for sustained (top row) and unsustained (bottom row) argon FRCs. Note the nonuniform timing of the figures.

dark bar oriented horizontally in the image, and the circular edge of the image is due to the edge of the window through which the camera looks. The breakdown of gas around the flux core is visible at 210 μs, and the beginning of merging is seen at 275 μs. The images at 300 and 325 μs show the bright central core of the FRC; in an unsustained case, the plasma light would continually decrease as the configuration decayed. The solenoid current begins to ramp at 320 μs, and by 425 μs, the plasma once again becomes quite bright. Note that the most intense light comes from the vicinity of the solenoid surface, where an X-point and divertor-like structure have formed (see Fig. 2, top row, t=425 μs). The plasma light then steadily decreases, slowly at first while the inductive voltage is applied, and then more quickly after the solenoid current has peaked and is crowbarred.

As implied in Fig. 2, field reversal is easily maintained when inductive current drive is applied to an argon FRC. This is demonstrated more clearly in Fig. 4, where the top row shows the midplane axial field profiles for sustained and unsustained discharges, as determined by the Spoke Probes. The field immediately after merging (325 μs) is identical for both cases, and field reversal is lost by 360 μs for the unsustained case. The sustained case, however, maintains field reversal throughout the solenoid current pulse. Note that the upturn in the axial field at small radius and late time is due to the leakage flux at the midplane gap between the solenoid coils, where positive axial field seeps out. The pressure profiles in the bottom row of Fig. 4 will be discussed below.

V. SUSTAINMENT ANALYSIS FOR INDUCTIVELY SUSTAINED DISCHARGES

The measurements made during sustained discharges in MRX allow an initial estimate of some FRC transport parameters. These estimates include the flux confinement time and the particle confinement time. It is important to stress from the beginning, however, that neither the plasma regime (low T_e, radiation dominated) nor the available measurements (lack of routine T_i measurements, noninvasive kinetic profiles) allow for a thorough study of transport.

These argon FRCs can be sustained for the duration of the solenoid current ramp, with the trapped flux either maintained or increased depending on the timing and voltage of the solenoid current pulse. This is illustrated in Fig. 5, where the results of a scan over the solenoid capacitor bank firing voltage (0, 5, 6, 7, 7.5, 8, 8.5, and 9 kV) at fixed fill pressure are illustrated; each curve represents the average of three similar discharges, and the grayed area on the far left indicates the period before merging is completed. The flux from the midplane solenoid flux loop is illustrated in Fig. 5(a), indicating the relative strength of the inductive drive. Figure 5(b) illustrates the poloidal flux trapped between the separatrix and the field null (ψ_t), as determined by the n=0 components from the spoke probes, while Fig. 5(c) shows the toroidal flux inside the separatrix. The poloidal flux is easily sustained by the solenoid, but the toroidal flux is near zero in all cases. The plasma thus maintains a pure FRC configuration equilibrium throughout the sustained phase. The surface voltage, defined as the time derivative of the separatrix poloidal flux, is shown in Fig. 5(d). The configuration is sustained as long as the surface voltage exceeds ~70 V. We also note that firing the solenoid earlier in the discharge results in a reduced loss of poloidal flux proceeding the sustained period, but also a reduced absolute configuration lifetime. The timing in Fig. 5 is optimal with respect to discharge duration.

The time traces illustrated in Fig. 5 show a second grayed region, between 400 and 430 μs, during which averages have been computed for analysis of the flux confinement. The results of this study are illustrated in Fig. 6, where all quantities are plotted as a function of the solenoid capacitor bank firing voltage. The trapped flux and surface voltage are illustrated in Figs. 6(a) and 6(b), respectively, showing the expected increases in these quantities with solenoid voltage. The flux confinement time is given by the ratio of the trapped flux (ψ_t) to the flux injection rate (the loop voltage, V_l), with a correction for the time derivative of the trapped flux:

Downloaded 21 Jul 2008 to 198.35.13.204. Redistribution subject to AIP license or copyright; see http://pop.aip.org/pop/copyright.jsp

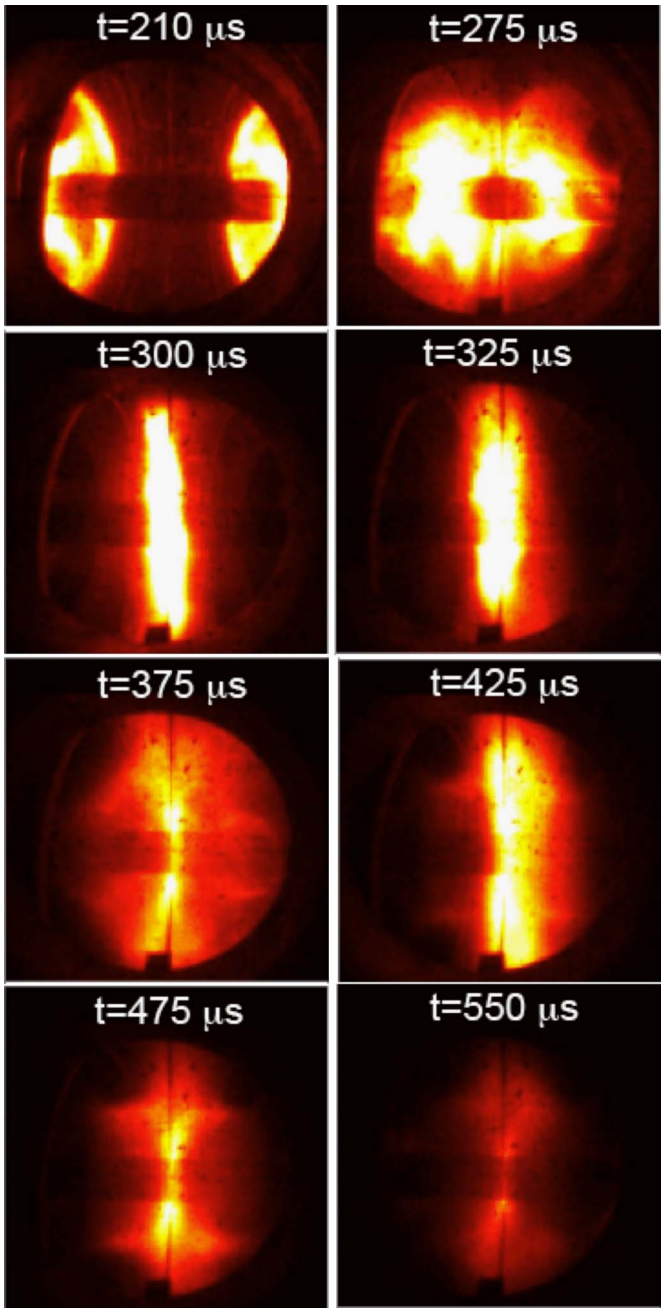

FIG. 3. (Color online) False color images of FRC formation and sustainment, taken in white light using a fast visible camera.

$$\tau_\phi = \frac{\psi_t}{V_l - d\psi_t/dt}. \tag{11}$$

This quantity is illustrated if Fig. 6(c), and shows a clear increase in the flux confinement with firing voltage. However, the increase can be largely explained through the larger minor radius with higher firing voltage ($\tau_\phi \propto \mu_0 a^2/\eta$),[72] as is demonstrated by normalizing the confinement time to the squared minor radius in Fig. 6(d). This result implies that the resistivity should be roughly constant as a function of the solenoid firing voltage. Note that the flux-loss correction ($d\psi_t/dt$) is typically less than 15% of V_l in this near steady-state phase of the discharges.

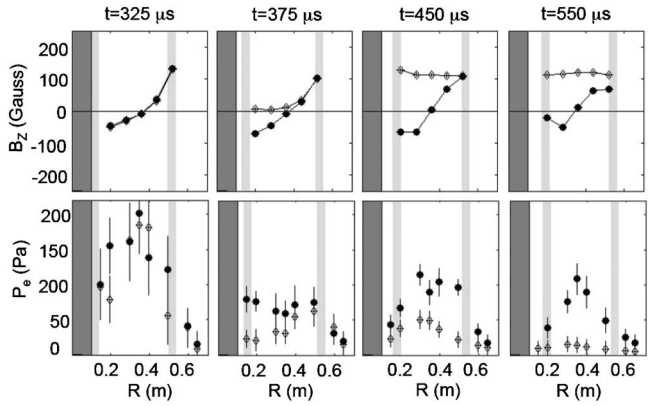

FIG. 4. Radial profiles of the axial magnetic field (top row), as measured by the spoke probes, and electron pressure (bottom row), as measured by radially scanning a Langmuir probe at the midplane. Results are shows for argon discharges with (closed symbols) and without (open symbols) inductive sustainment.

The data in Fig. 6(e) show a comparison between two determinations of the plasma resistivity. The measured resistivity comes from the measured toroidal electric field and toroidal current density as $\eta^* = \int E_\phi dV / \int J_\phi dV$, where the integrals are over the plasma volume. The Spitzer resistivity is calculated as[73]

$$\eta_\perp = 1.03 \times 10^{-4} T_e^{-3/2} Z_{\text{eff}} \ln \Lambda. \tag{12}$$

The T_e in the calculation is measured at the center of the FRC with the Langmuir probe; radial scans of the Langmuir probe have indicated that the T_e profile is flat in these plasmas, so that the central value is largely indicative of the bulk value. Not having an independent measure of Z_{eff}, a value $Z_{\text{eff}}=1.5$ is assumed in the calculation. The electron temperature in measured by the Langmuir probe at $R=0.35$ m for all cases, and is found to be largely independent of firing voltage, likely due to the (presumably) large radiated power in argon plasmas. The agreement between the two resistivity measurements is surprisingly good, illustrating that the flux decay in these low-temperature plasmas is likely classical, though uncertainties in the determination of $\eta_\perp$ prevent an absolute conclusion of classical resistivity. For instance, if $Z_{\text{eff}}=1.0$, then the resistivity would be overestimated by $\sim$30% and some slight resistivity anomaly might be present (note that $Z_{\text{eff}} \geqslant \sim 1.7$ is apparently excluded, as the collisional resistivity would then unphysically exceed the measured values). A finding of classical resistivity would be in keeping with other results from higher-density plasmas in MRX.[73,74] Note that theta-pinch and RMF formed prolate FRCs, which have significantly different plasma parameters than the present experiments, often have resistivities much larger than classical.[75]

In addition to the electron-ion collisions that lead to the Spitzer resistivity, electron-neutral collisions can contribute to the plasma resistivity. The momentum transfer rate coefficient for electron-neutral collisions in argon is approximately $\langle \sigma v \rangle_{\text{en}} \approx 1.67 \times 10^{-7}$ cm^3/s.[76] Assuming a neutral density equal to the plasma density (1×10^{14} cm^{-3}) yields a collision rate of 1.7×10^7 s^{-1}. The consequent resistivity can

Downloaded 21 Jul 2008 to 198.35.13.204. Redistribution subject to AIP license or copyright; see http://pop.aip.org/pop/copyright.jsp

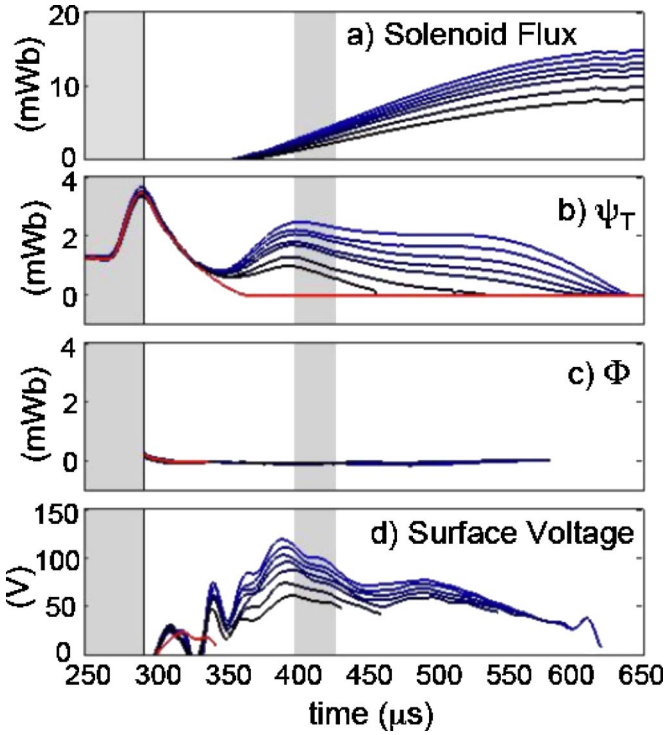

FIG. 5. (Color online) Scan over solenoid firing voltage with all other parameters (fill pressure, coil waveform shapes) held fixed. Shown are the (a) solenoid flux, (b) trapped poloidal flux, (c) toroidal flux, and (d) surface voltage. The short-lived plasma in frame (b) is a case without sustainment. The gray areas on the far left represent the time before merging is finished, and those near 410 μs represent the time duration for the averages in Fig. 6.

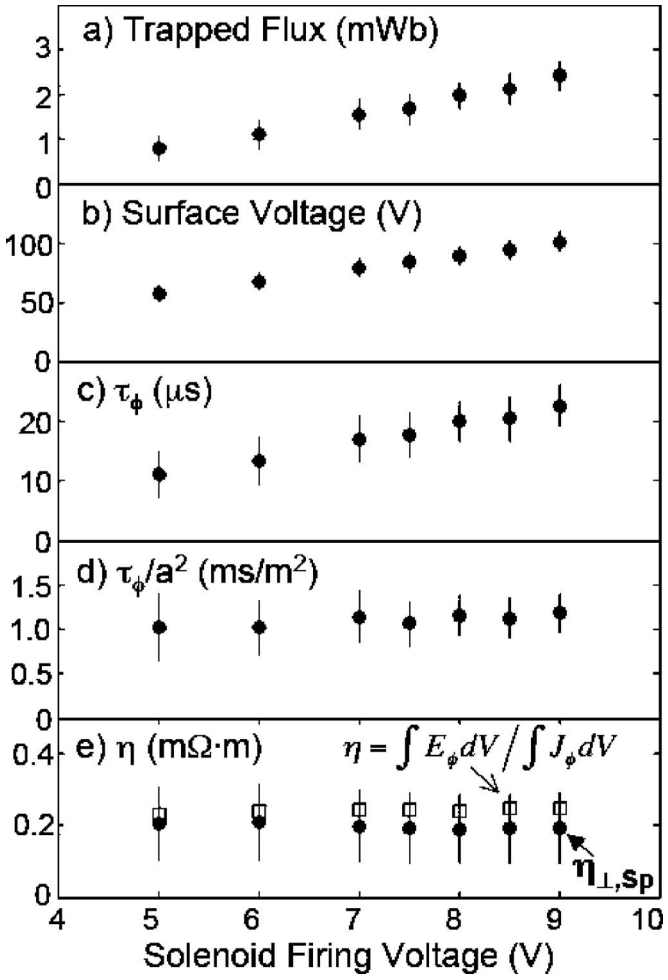

FIG. 6. Measured and derived plasma parameters as a function of solenoid firing voltage, for the argon FRC voltage scan in Fig. 5. The data are averaged over the period 400–430 μs, and error bars represent shot-to-shot variability.

be estimated as $\sigma_{en}=m_e\nu_{en}/e^2n_e \approx 0.007\ \mathrm{m\Omega\cdot m}$. Hence, resistivity due to electron-neutral collisions is a small contribution to the total, even assuming a large neutral density (see discussion below regarding neutral penetration).

The particle and magnetic flux balance in an FRC can be understood from the use of Ohm's law (here V is the single-fluid velocity),[57]

$$\vec{E}+\vec{V}\times\vec{B}=\eta_\perp\vec{j}. \tag{13}$$

The perpendicular resistivity was shown above to be well approximated by the simple Spitzer resistivity in these plasmas, though some phenomenological resistivity that incorporates the effect of turbulence might be appropriate in other contexts. Taking the toroidal component of this equation leads to

$$V\cdot\nabla\psi = R\eta_\perp J_\phi - RE_\phi \tag{14}$$

and integrating over the magnetic surface yields an expressions for the net particle flux across the surface as

$$\Gamma(\psi)=n(\psi)\eta_\perp(\psi)\left[\left((2\pi)^2\int R^2\frac{ds}{B}\right)\right]\frac{\partial P}{\partial\psi}-n(\psi) \times\left[2\pi\int(RE_\phi)\frac{ds}{B}\right]. \tag{15}$$

In this expression, s is the length along to poloidal magnetic field contour, and $n(\psi)$ is the plasma density. The first term on the right-hand side represents outward classical diffusion, while the second term represents an inward pinch of particles. In steady state, the diffusion (of particles and magnetic flux) is balanced by a constant inward flux. Because the diffusion is proportional to the pressure gradient, the pressure will build until the diffusive term balances the pinch. Note that the same formulation describes the evolution of unsustained FRCs (either prolate or oblate) if E_φ is set to zero.[57]

This peaking of the pressure gradient and balance of the particle fluxes has been studied during inductive sustainment (7.5 kV solenoid voltage in this case). Radial scans of the triple Langmuir probe were conducted over many repeatable discharges, in order to measure profiles of the electron temperature and density; these profiles are shown in the bottom row of Fig. 4. The electron pressure immediately after merging (325 μs) is quite high, but begins to quickly decay. By 375 μs, the pressure in the unsustained case has dropped, while that in the sustained case shows the first response to the induction. The sustained pressure profile then reacquires its peaked shape, maintaining that peaked structure throughout the sustained period. Note that because the electron tem-

Downloaded 21 Jul 2008 to 198.35.13.204. Redistribution subject to AIP license or copyright; see http://pop.aip.org/pop/copyright.jsp

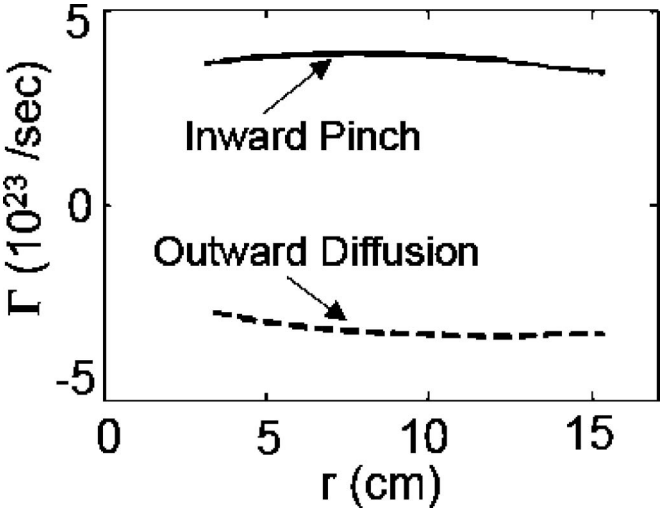

FIG. 7. Profiles of the radial particle flux, as determined by the Ohm's law analysis.

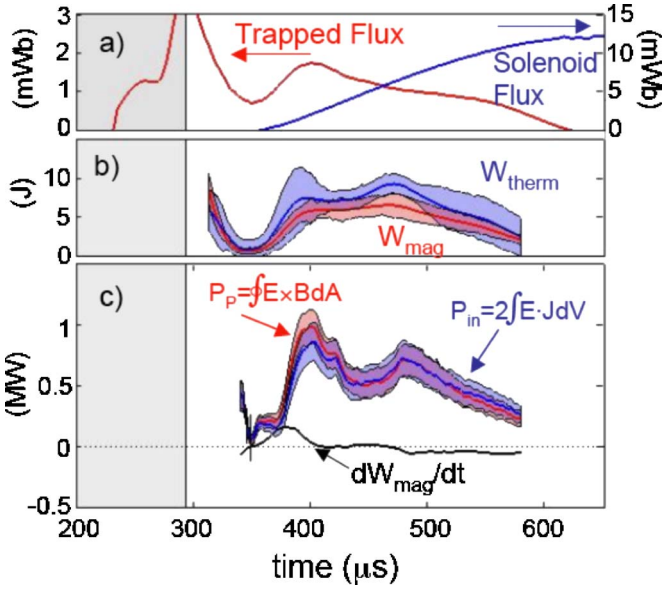

FIG. 8. (Color online) Time evolution of (a) the trapped poloidal flux and the solenoid flux, (b) the total thermal and magnetic energies, and (c) the terms in the Poynting's theorem power balance analysis.

perature profile is largely flat and constant in time during these sustained discharges, the profiles plotted here are largely indicative of the density profiles.

It is implicit in this picture of sustainment that the ionization source of plasma occurs outside the FRC separatrix, so that the plasma is brought in by $E \times B$ motion. The electron-impact ionization rate coefficient for argon is approximately $\langle \sigma v \rangle = 10^{-8}$ cm^3 s^{-1} for a $T_e = 7$ eV argon plasma.[76,77] Taking a measured plasma density of 10^{13} cm^{-3} outside the separatrix, corresponding to one-tenth of the peak density, yields an ionization rate of 100 kHz. Assuming that the neutral argon is at room temperature, and is thus incoming with a velocity of 350 m/s, the mean free path for ionizing collisions is 3.5 mm. Hence, even allowing for large errors in these approximations, it is clear that very little neutral argon should be able to penetrate past, or even to, the separatrix.

The precise evaluation of the individual terms in Eq. (15) is difficult, due to imperfect knowledge of the profiles $n(\psi)$, $dP/d\psi$, and $\eta_\perp(\psi)$. However, approximate calculations of the inward and outward particle flux are shown in Fig. 7 for the profiles at 475 μs for the 7.5 kV solenoid voltage discharges. To evaluate the fluxes, the measured midplane density profile was mapped to poloidal flux, yielding an approximate $n(\psi)$. The resistivity $\eta_\perp(\psi)$ was estimated as $\eta_\perp(\psi) = \langle E_\varphi \rangle / \langle J_\varphi \rangle$, where $\langle \ldots \rangle$ implies an average over the magnetic surface (or field line in this case), and E_φ was determined from the poloidal flux change as per Eq. (5). As indicated in Fig. 6, this resistivity is typically equal to the Spitzer resistivity to within 30% when $Z_{\text{eff}} = 1.5$ is assumed. Finally, the pressure, and then the pressure gradient, were determined from force balance, based on the measured magnetic field profiles. The resulting profiles of the particle flux illustrate the approximate consistency between the inward pinch flux and the outward diffusive flux. The total particle inventory can be roughly estimated from the mapping of density to poloidal flux, yielding a total particle inventory of $\sim 1 \times 10^{19}$. The inward flux of $\sim 4 \times 10^{23}$ s^{-1} yields a crude estimate of the particle confinement time during this roughly steady-state phase of 25 μs. This is approximately similar to the flux-confinement time, though the particle confinement estimation is too crude to warrant detailed comparisons.

The final quantity of confinement interest is the energy confinement time, calculated as

$$\tau_E = \frac{W_{\text{therm}}}{P_{\text{in}} - \partial W_{\text{therm}}/\partial t}. \tag{16}$$

The stored thermal energy (W_{therm}) can be estimated from the pressure profile, as determined from force balance. The input power (P_{in}) can be derived from Poynting's theorem[78] as

$$P_P = \frac{dW_{\text{mag}}}{dt} + P_{\text{in}}, \tag{17}$$

$$P_P = \oint \vec{E} \times \vec{B} dA, \tag{18}$$

$$P_{\text{in}} = 2 \int E \cdot J dV. \tag{19}$$

The term P_P represents power flowing across the separatrix, and can be simplified to $I_T V_l$ when the plasma boundary is stationary[79] (I_T is the toroidal current and V_l is the loop voltage). The version in Eq. (18) will be used in this paper, however, to account for the dynamic boundary shape change when the solenoid is energized. The first term on the right-hand side of Eq. (17) measures the increase in stored magnetic energy. The second term on the right-hand side indicates power input to the plasma. This power can either increase the stored thermal energy of the plasma or be lost through transport or radiation.[80]

The various terms in this expression are illustrated for a typical discharge in Fig. 8, for a discharge for 7.5 kV solenoid voltage (discharges with larger firing voltages tended to

Downloaded 21 Jul 2008 to 198.35.13.204. Redistribution subject to AIP license or copyright; see http://pop.aip.org/pop/copyright.jsp

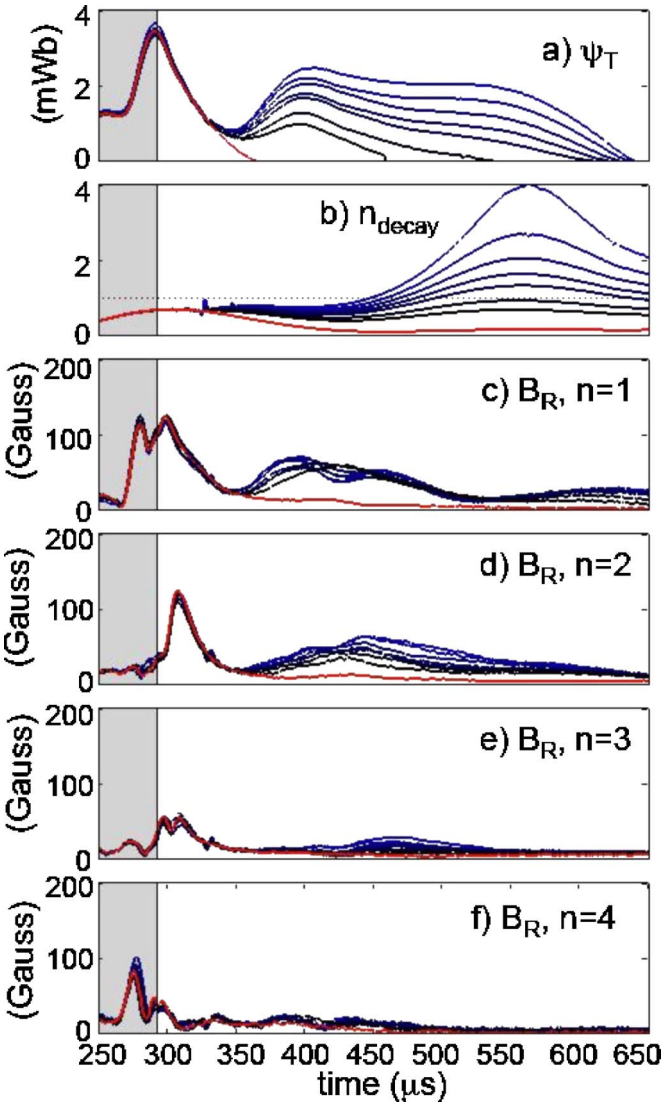

FIG. 9. (Color online) Poloidal flux, decay index (n_{decay}), and midplane B_R perturbations as a function of time, in argon plasmas sustained with different solenoid voltages.

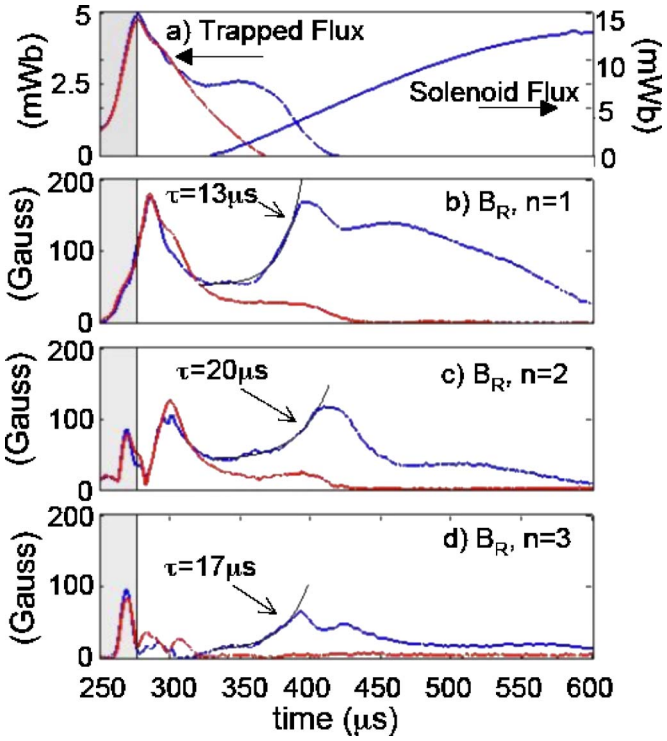

FIG. 10. (Color online) (a) The trapped flux and solenoid flux, and (b)–(d) the nonaxisymmetric B_R perturbations, for sustained and unsustained nitrogen discharges.

have a separatrix which crossed the large R boundary of the Large Area Array, and the surface integral in Eq. (18) could not be computed in this case). The waveforms of the solenoid flux and trapped poloidal flux are illustrated in Fig. 8(a), showing the increase in poloidal flux with induction, followed by a period of approximate sustainment. The thermal and magnetic energies inside the separatrix are shown in Fig. 8(b), along with error regions. The dominant source of error for the magnetic energy calculation comes from uncertainty in the determination of the separatrix flux, given that the magnetic energy is concentrated at the FRC edge; the uncertainty in the thermal energy is estimated by repeating the calculation in Eq. (8) from the left and right side of the array when estimating the pressure, and taking the difference between them to estimate the error. The input power shows a peaking at 1 MW, then lowers to a more steady level of 600 kW. The dissipated power essentially follows the input power, except for some difference at the beginning of the solenoid current ramp and during the decay of the plasma. Although these differences are comparable to or smaller than the uncertainties, it is worth noting that they are similar to the rate of change in the stored magnetic energy. The energy confinement time during the period of steady sustainment can be very crudely estimated as $\tau_E \sim 7\ J/600\ \text{kW} = 11\ \mu\text{s}$. Note, however, that the (presumably) large radiated power in this argon plasma precludes drawing any general conclusions about the energy transport in a sustained oblate FRC.

VI. STABILITY OF FRCs UNDER INDUCTIVE SUSTAINMENT

As noted above, the sustainment of argon and krypton FRCs in MRX is typically not limited by any instability. This is not the case in discharges formed in lighter gases, such as deuterium and helium, where rapid instability terminates the configuration. This section addresses the stability of these plasmas by considering the stabilizing effects of equilibrium field shaping, magnetic diffusion, and finite-Larmor radius effects.

The stability features of argon discharges are illustrated in Fig. 9. The top frame shows the trapped poloidal flux for the same voltage scan as illustrated in Fig. 5. The $n=1$ (tilt) and 2 midplane B_R perturbations, illustrated in Fig. 9(c) and 9(d), shows some mode growth during the initial sustainment period. Both of these modes saturate, and then begin to decrease long before the end of sustainment. The $n=3$ and 4 modes show essentially no growth throughout the discharges, even though there are sizeable perturbations from which an instability could grow.

Downloaded 21 Jul 2008 to 198.35.13.204. Redistribution subject to AIP license or copyright; see http://pop.aip.org/pop/copyright.jsp

TABLE I. Typical range of parameters for FRCs in MRX. Some discharges lay outside the typical range specified here.

	Deuterium	Helium	Nitrogen	Neon	Argon	Krypton
Mass	2	4	14	20	40	84
Density (10^{19} m^{-3})	4–10	2.5–6	8–16	4–9	7–13	8–13
T_e (eV)	7–10	8–10	4.5–7	7.5–9	6–8	4.5–5.5
$B_{Z,Sep}$ (G)	180–280	150–200	130–170	160–200	100–160	130–145
V_A (km/s)	25–50	25–50	6–10	10–16	3–5	1.5–2.5
$\tau_A = a/V_A$ (μs)	3.5–7	3–8	16–33	9–17	35–55	75–110
$S = \mu_0 a V_A/\eta$	50–150	50–150	6–10	15–30	2–6	1–2
T_i (eV)	10 ± 4	10 ± 4	8 ± 3	10 ± 3	8 ± 4	9 ± 4
$\bar{s}$	1–3	1–3	0.9–1.1	0.45–0.8	0.2–0.5	0.1–0.2

The stable sustainment typically observed in argon plasmas does not transfer to other gases. An example of this is illustrated in Fig. 10, where the results from sustained and unsustained N_2 discharges are illustrated. The sustained case exhibits an ≈ 50 μs period of steady flux, but then collapses long before the end of the solenoid current ramp. This collapse is proceeded by the growth of midplane magnetic perturbations; the growth time of 13–20 μs is similar to the Alfven time $\tau_A = a/V_A = 20$ μs. These perturbations have the signature of the axially polarized co-interchange instability, which have previously been found to terminate the FRC plasma in both simulation[39] and experiment.[46] Note that the $n=1$, 2, and 3 modes grow simultaneously, making it impossible to assign the final collapse to any one mode. This particular sustained discharge displayed clear mode growth, enabling a clear estimation of the growth times. However, many deuterium, helium, nitrogen, and neon discharges showed a more complicated pattern of rapid yet unsteady and complicated perturbation growth, making it very difficult to calculate the growth rates of particular modes.

Many sets of discharges have been taken in deuterium, helium, nitrogen, neon, argon, and krypton, and the results have been combined into a small database. Groups of three to six similar shots were combined to form a single data point. All discharges in the database had at least 7 kV of solenoid capacitor bank voltage, and the inductance and capacitance of the solenoid circuit were identical for all cases. The external field time evolution was also quite similar, and was strongly influenced by the solenoid/compensation coil combination once the solenoid current began to ramp. Some basic parameters of these different plasmas are presented in Table I. The ion temperature is an important parameter in assessing how kinetic the plasma is; there was not, however, an ion temperature measurement for every discharge. For the calculations described below, a single ion temperature was utilized for each species, as determined from the known total pressure (from magnetics) and the electron temperature and density (from the Langmuir probe) for typical discharges. This value was checked against that measured via Doppler broadening in a limited number of cases, and agreement was found within large error bars. The resulting ion temperatures, along with the associated uncertainties, are provided in Table I. These uncertainties are propagated through all expressions that rely on the ion temperature, and are reflected in the error bars for all plots below. Note that $T_i > T_e$ in some cases is likely due to the initial ion heating during the merging phase, as demonstrated in MRX[47] and TS-3.[81]

Analysis of the database indicates the anticipated strong correlation between the lifetime and the amplitude of nonaxisymmetries, as illustrated in Fig. 11. The lifetime is defined as the time between the end of spheromak merging and the time when the poloidal flux decreases to 10% of its maximum value. The B_R perturbations are measured by the Spoke Probe coils at $R=0.28$ cm, and are normalized to the separatrix B_Z field at the end of merging. As noted in Sec. III, these B_R perturbations are indicative of the plasma perturbations associated with the axially polarized co-interchange instability.

A quick glance at the figure illustrates that the lifetimes of deuterium (magenta) and helium (red) FRCs are always

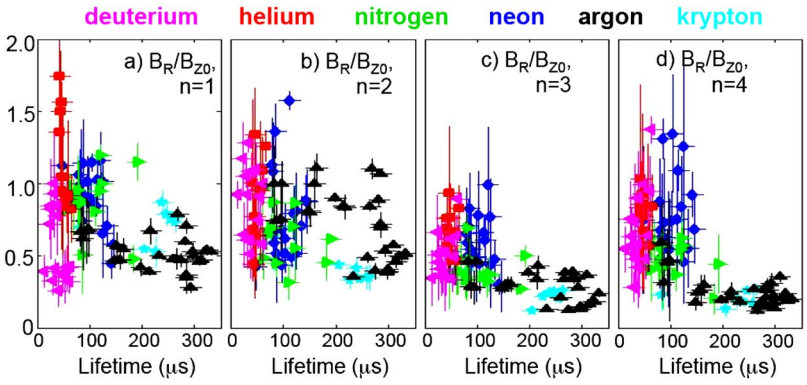

FIG. 11. (Color online) The maximum amplitude of B_R $n=1$, 2, 3, and 4 modes, normalized by the B_Z field at the separatrix immediately after merging, plotted against the FRC lifetime for a range of working gases.

Downloaded 21 Jul 2008 to 198.35.13.204. Redistribution subject to AIP license or copyright; see http://pop.aip.org/pop/copyright.jsp

much less than the 300 μs long solenoid current ramp. These plasmas show large nonaxisymmetries during and immediately after merging, which grow and ultimately terminate the configuration. The solenoid current timing in these light-gas cases was often adjusted to provide a one-turn voltage at the end of the merging phase, through this seldom resulted in any appreciable period of sustainment. The nitrogen (green) and neon (blue) plasmas show some period of sustainment when the induction is applied, before eventually succumbing to instabilities. The data in Fig. 11 show that these short-lived plasmas typically have large magnetic perturbations. Further database analysis (not shown) demonstrates that the time of maximum instability amplitude almost always occurs as the discharge collapses, and that as illustrated in Fig. 10, the perturbations with different toroidal mode numbers typically peak at similar times in these unstable discharges. Note finally that $n=4$ is the largest mode number that can be resolved with the present array. When large mode amplitudes are observed for all n, it cannot be excluded that $n>4$ modes are spatially aliasing into lower-n perturbations.

The argon (black) and krypton (cyan) plasmas, however, are typically sustained for the entire 300 μs length of the solenoid current ramp. As noted above and shown in Figs. 11(a) and 11(b), these plasmas often display some $n=1$ and 2 modes as the poloidal flux is ramped up, resulting in temporarily large amplitude perturbations which then decay. There are only small $n=3$ and 4 perturbations in these cases. The outstanding issue is then to understand why only these two gases allow sufficient stability for long-time sustainment. In the discussion below, three different stabilization effects are shown to be important.

A. Stabilizing effect no. 1: Equilibrium field shaping

For the $n=1$ (tilt) mode in argon, the observed stability is at least partly explained by the time evolution of the external field throughout the solenoid current ramp. The stability to the tilt-mode can be approximately evaluated through a rigid-body model.[82] A quantity known as the decay index (n_{decay}) is defined as

$$n_{\mathrm{decay}} = -\frac{R}{B_Z}\left[\frac{\partial B_Z}{\partial R} - \frac{Z}{R^2}\frac{\partial}{\partial R}(2RB_R + ZB_Z)\right]. \qquad (20)$$

This quantity is calculated based on the field caused by all coils and their associated vacuum vessel image currents. If the plasma begins to develop a rigid-body tilt, there is a resulting torque in the direction of the initial tilt whose magnitude is proportional to $(1-n_{\mathrm{decay}})$. Hence, $n_{\mathrm{decay}}>1$ provides stability to a rigid-body tilt. The solenoid/compensation coil combination was arranged such that $n_{\mathrm{decay}}>1$ once the solenoid flux exceeded ~3 mWb. This is illustrated in Fig. 9(b), where the transition to $n_{\mathrm{decay}}>1$ corresponds to the time when the $n=1$ modes begin to decrease in amplitude. The FRCs formed in lighter gases typically succumb to instability before n_{decay} exceeds 1, and are thus tilt-unstable throughout their (brief) lifetime. Given that the tilt-instability is simply the n=1 version of the axially polarized co-interchange, we anticipate from theory[39,46] and experiment[46] that the transition to $n_{\mathrm{decay}}>1$ will also somewhat improve the stability of the $n=2$ mode. Note that the calculation of n_{decay} utilized flux-conserving Green's tables[83,46] that automatically incorporate the effects of (toroidal) eddy currents in the vacuum vessel wall.

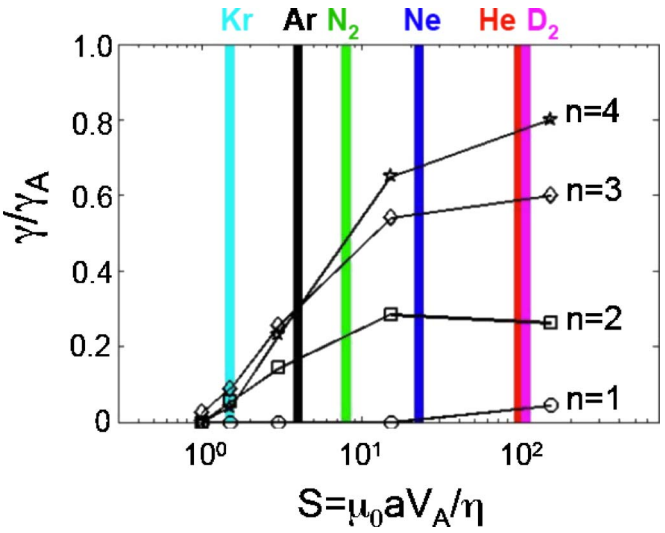

FIG. 12. (Color online) Growth rates for the $n=1$, 2, 3, and 4 axially polarized co-interchange modes, as a function of Lundquist number. The vertical lines show the typical Lundquist numbers of the different working gases.

The stability to $n=3$ and 4 modes cannot be so easily explained by the equilibrium field shaping. Previous simulations,[39] in addition to those presented below, demonstrate that these modes are not effectively stabilized by plasma shaping, and the apparent stability thus must lie outside of ideal MHD. Two likely stabilizing effects are magnetic diffusion and finite-Larmor radius stabilization.

B. Stabilizing effect no. 2: Magnetic diffusion

Magnetic diffusion, due to plasma resistivity, can stabilize the instability by dissipating the perturbed currents that drive the instabilities. The key governing parameter for global ideal modes is the ratio of the resistive diffusion time ($\sim a^2\mu_0/\eta$) to the Alfven time (a/V_A), also known as the Lundquist number and defined here as $S=\mu_0 a V_A/\eta$. In order to assess the effect of resistivity on the stability properties of these plasmas, linearized simulations of the $n=1$, 2, 3, and 4 modes were performed using the HYM code.[30] The calculations were initiated with Grad-Schafranov MHD equilibria[84] computed with the MRXFIT code,[46] for an argon plasma during the middle of the sustainment phase ($t=475$ μs). A perturbation with both radial and axial components was applied to the plasma, and the growth rate of the fastest growing mode was calculated. The procedure was repeated for different toroidal mode numbers and resistivities (and hence S). In order to mock-up the inductive sustainment, the axisymmetric part of the resistivity was set to zero in these calculations, but resistivity was kept for perturbed currents. This resistivity was then scanned to evaluate its impact on the mode growth rate. The fastest growing mode was always an axially polarized mode; the growth rates for these modes are illustrated in Fig. 12, with vertical lines indicating the typical

Downloaded 21 Jul 2008 to 198.35.13.204. Redistribution subject to AIP license or copyright; see http://pop.aip.org/pop/copyright.jsp

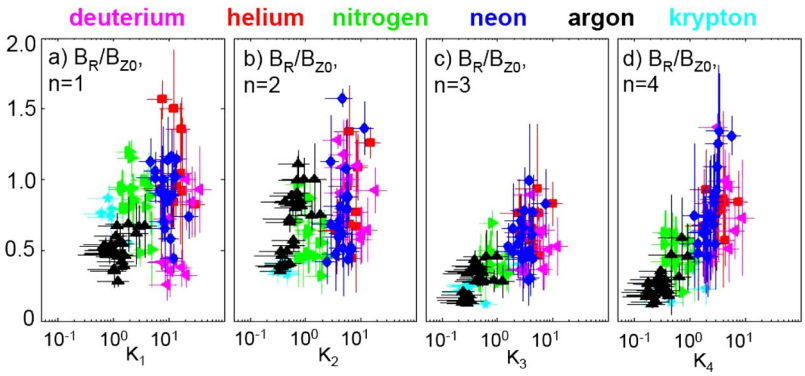

FIG. 13. (Color online) Amplitude of the B_R perturbations, as a function of the kinetic stability parameters K_n, $n=1$, 2, 3, and 4.

Lundquist numbers of different FRCs in MRX.

The $n=1$ mode is essentially stabilized for all resistivities, as anticipated based on the rigid-body analysis. This stabilizing effect is due to the shaping of the equilibrium field and is present in ideal MHD, as evidenced by the very small growth rate at $S=100$. This stabilizing factor should only be present when the solenoid current ramp has begun and $n_{\text{decay}}>1$; the period before the solenoid has fired has $n_{\text{decay}}\approx 0.5$, and is expected and observed to be $n=1$ unstable.

For ideal MHD (large S), the simulated growth rate increases with toroidal mode number. This has been observed before and is related to a reduction in stabilizing field-line bending[36] as n is increased; the most unstable modes in ideal MHD are those with $n\rightarrow\infty$.[30,36,39] However, the growth rates show a strong decrease as S is reduced, and the $n=4$ growth rates at small S are actually smaller than for $n=3$. This can be understood by noting that resistive dissipation scales as ηk^2, where k has both radial components ($k_R\sim 1/a$) and toroidal components ($k_\phi\sim n/R$). For $n=1$, 2, and 3, k_R is larger than or comparable to k_ϕ, and dominates the dissipation. For $n=4$ and above, the dissipation from k_ϕ dominates. The growth of modes with $n>4$ will be even more strongly suppressed, because the $k^2\sim n^2$ scaling of the dissipation is stronger than the $\gamma\propto n$ (or weaker) scaling[39] of the co-interchange growth rate. From a practical point of view, the reduced growth rates at krypton-like Lundquist number ($S\approx 1.5$) strongly imply that magnetic diffusion alone can account for the stability of krypton plasmas.

Finally, for argon-like Lundquist numbers ($S=4$), the growth rates for the $n=2$, 3, and 4 modes are 0.17, 0.3, and 0.3, respectively. The argon plasmas often live for $(6-7)\tau_A$, or >2 growth times for the $n=3$ and 4 modes; this is sufficient for a factor of $e^2\approx 7$ increase in the mode amplitude. Furthermore, there were sizeable perturbations present during the merging process and early solenoid current ramp, which provide a seed from which the instability could grow. However, no growing $n=3$ and 4 modes were observed. This result strongly implies that additional stabilizing effects are present. The results presented next show that FLR physics likely plays an important role in stabilizing these modes for the argon case.

C. Stabilizing effect no. 3: Finite-Larmor radius stabilization

In order to test the hypothesis that FLR stabilization physics is important in stabilizing the $n=3$ and 4 modes in these argon FRCs, the instability amplitudes are plotted against the parameter K_n in Fig. 13. Here, the kinetic parameter is defined as $K_n=1/2\gamma_A/\omega^*$, where $\omega^*=nT_i/R_0aB_{Z,\text{sep}}$ is proportional to the toroidal mode number n (i.e., $k\sim n/R_0$ and the gradient scale length is taken to be the minor radius a). The factor of $\frac{1}{2}$ in K_n is an attempt to account for the observation that the predicted growth rates of most modes in MRX are typically $\approx\gamma_A/2$. This is borne out by the calculations presented in Fig. 12 for the equilibrium when the solenoid is energized. For the He and D_2 cases where the instabilities grow before the solenoid is energized, the growth rates should be similar to the mirror-ratio 2.8–3.5 cases discussed in Ref. 46, where the growth rates were also typically a fraction of the inverse Alfven transit time.

As anticipated from the discussion of equilibrium field effects above, the $n=1$ and 2 amplitudes are not strong functions of the relevant kinetic parameters (K_1 and K_2); this fits expectations because both kinetic parameters are >1 for essentially all plasmas in the database. The $n=3$ and 4 mode amplitudes, however, show a strong scaling with the parameters K_3 and K_4. When these parameters are <1 and strong kinetic effects are expected, these modes are stabilized. For plasmas with K_3 and $K_4\gg 1$, large modes with those mode numbers are observed to grow. It is especially important to note that there are a small subset of argon plasmas with slightly larger values of K_3 and K_4, and that these plasmas do indeed develop the associated instabilities. Taken in totality, these results provide strong evidence for the role of FLR effects in stabilizing the co-interchange mode in an oblate FRC plasma.

These results confirm to some extent the prediction in Belova *et al.*[39] that thermal FLR effects are less efficient in stabilizing pressure-driven modes in oblate FRCs, compared to the prolate case. For typical prolate FRCs with elongations of 4–10, a value of $\bar{s}=2$ is sufficiently small to place the plasmas in the kinetic regime ($\bar{s}/E<\sim 0.5$). If this criterion is applied to the FRCs in this paper with elongations of ~ 0.5, the required $\bar{s}$ is in the range of 0.25, which is only obtained in the sustained krypton and argon plasmas. Only

Downloaded 21 Jul 2008 to 198.35.13.204. Redistribution subject to AIP license or copyright; see http://pop.aip.org/pop/copyright.jsp

for higher-n modes ($\omega^* \propto n$) are FLR effects important for oblate FRCs in MRX, even though $\bar{s}$ is fairly small by prolate FRC standards.

VII. DISCUSSION AND CONCLUSIONS

The results presented in this paper demonstrate the stable sustainment of oblate FRC plasmas for times much longer than the magnetic diffusion time. A summary of the results can be provided as follows:

(i) Argon and krypton oblate FRC plasmas have been sustained for up to 350 μs with inductive current drive. The best examples are sustained for >15 flux confinement times or >6 Alfven times, with trapped flux levels above 2.5 mWb.

(ii) The method of sustaining the FRC equilibrium in these plasmas has been elucidated. The configuration is maintained as a balance between an inward $E \times B$ pinch and outward diffusion. The classical outward diffusion is proportional to the plasma resistivity, which is typically close to the collisional Spitzer resistivity in these stable argon plasmas, though large uncertainties preclude a more systematic analysis. This mechanism is directly analogous to the resistive decay of a prolate FRC,[57] but with the addition of the inward pinch.

(iii) The stability in argon oblate FRCs does not transfer to lighter gases. The lightest gases (deuterium and helium) often collapse due to instability even before the solenoid current ramp begins; the period of sustainment is quite short. Moderate weight gases (N_2 and Ne) typically show a period of sustainment before the growth of terminal instabilities. In all these cases, the instabilities have the characteristics of the axially polarized pressure driven co-interchange instability.

(iv) Three effects are important in maintaining stability through the solenoid current ramp in the argon and krypton plasmas. The equilibrium field configuration (field index) during the ramp helps to stabilize the dangerous $n=1$ tilt instability in a fashion specific to the oblate FRC. Magnetic diffusion can assist in stabilizing all modes when the Lundquist number is sufficiently low ($S<2$). FLR physics is observed to stabilize $n=3$ and 4 modes in sufficiently kinetic plasmas. When the FRC does not benefit from any of these effects (the typical helium and deuterium plasmas, for instance), rapid and destructive instabilities are observed to occur. These last two effects are generally applicable to the oblate or prolate FRCs.

The difficulty in sustaining light-gas oblate FRCs in the present experiment should not be interpreted in an overly pessimistic way. These experiments were conducted without either flexible shape control or nearby passive stabilizers. Previous studies of decaying FRCs in MRX showed that proper shaping of the equilibrium field could lead to FRCs with improved stability.[46] These discharges maintained $n_{\mathrm{decay}}>1$ for the entire discharge duration; a more sophisticated poloidal field system, with additional coils and power supplies, would allow $n_{\mathrm{decay}}>1$ for the entire period after merging for these sustained plasmas as well. A second result from previous MRX research indicated the importance of nearby conducting stabilizers in stabilizing $n=1$ modes. The incorporation of a segmented conducting shell in the solenoid assembly, outside the solenoid windings but inside the vacuum liner, or conducting shells on the outboard side of the plasma, would allow for passive stabilization of inductively sustained plasmas.

Plasma shaping and nearby passive stabilizers, along with spheromak merging and neutral beam injection (NBI), are key components of the SPIRIT oblate FRC concept.[47] The FRC in this case would be formed via spheromak merging; conducting shells would be utilized to stabilize low-n modes during the merging and FRC stages of the discharge. NBI would then be applied, fulfilling two important functions. First, the NBI would assist with plasma current sustainment, as described in Sec. II. Second, FLR effects from the energetic ions would provide stabilization to co-interchange instabilities. Indeed, simulations have found sustained configurations that are stable to all low-n MHD modes when energetic beam ions and conducting shells are utilized.[43,47] A target plasma of sufficient poloidal flux level and electron temperature is required to make NBI feasible. In order the achieve this target plasma in an MRX scale device, a solenoid will be utilized to both provide Ohmic heating in non-radiation-dominated plasmas and to increase the FRC flux level. The experiments described in this paper provide a step toward realizing this approach to oblate FRC development.

ACKNOWLEDGMENTS

The authors would like to thank Dave Cylinder for assistance constructing the magnetic probes used in these experiments, and Robert Cutler for his work in maintaining and upgrading all aspects of the MRX facility. We also wish to thank the PPPL engineering and technical staff, including Don McBride, Doug Loesser, Jim Chrzanowski, Frederick Simmonds, Frank Terlitz, and Mike Hauss, for their work in the design and construction of the solenoid system. The work benefited from useful discussions with Y. Ono and Y. Raitses.

This work was funded by the U.S. Department of Energy.

[1] M. Tuszewski, Nucl. Fusion **28**, 2033 (1988).
[2] H. Momota, A. Ishida, Y. Kohzaki, G. H. Miley, S. Ohi, M. Ohnishi, K. Yoshikawa, K. Sato, L. C. Steinhauer, Y. Tomita, and M. Tuszewski, Fusion Technol. **21**, 2307 (1992).
[3] H. Himura, A. Okada, S. Sugimoto, and S. Goto, Phys. Plasmas **2**, 191 (1995).
[4] H. Y. Guo, A. L. Hoffman, K. E. Miller, and L. C. Steinhauer, Phys. Rev. Lett. **92**, 245001 (2004).
[5] J. T. Slough and A. L. Hoffman, Phys. Plasmas **6**, 253 (1999).
[6] A. L. Hoffman, P. Gurevich, J. Grossnickle, and J. T. Slough, Fusion Technol. **36**, 109 (1999).
[7] E. Kawamori and Y. Ono, Phys. Rev. Lett. **95**, 085003 (2005).
[8] A. F. Lifschitz, R. Farengo, and N. R. Arista, Nucl. Fusion **42**, 863 (2002).
[9] A. F. Lifschitz, R. Farengo, and A. L. Hoffman, Nucl. Fusion **44**, 1015 (2004).
[10] H. A. Blevin and P. C. Thoneman, Nucl. Fusion Suppl. **1**, 55 (1962).
[11] P. M. Bellan, Phys. Rev. Lett. **62**, 2464 (1989).
[12] I. R. Jones, Phys. Plasmas **6**, 1950 (1999).
[13] A. L. Hoffman, Nucl. Fusion **40**, 1523 (2000).
[14] J. T. Slough and K. E. Miller, Phys. Rev. Lett. **85**, 1444 (2000).
[15] R. D. Milroy, Phys. Plasmas **7**, 4135 (2000).
[16] S. A. Cohen and R. D. Milroy, Phys. Plasmas **7**, 2539 (2000).

Downloaded 21 Jul 2008 to 198.35.13.204. Redistribution subject to AIP license or copyright; see http://pop.aip.org/pop/copyright.jsp

[17] A. L. Hoffman, H. Y. Guo, R. D. Milroy, and Z. A. Pietrzyk, Nucl. Fusion **43**, 1091 (2003).
[18] R. D. Milroy and K. E. Miller, Phys. Plasmas **11**, 633 (2003).
[19] H. Y. Guo, A. L. Hoffman, R. D. Milroy, K. E. Miller, and G. R. Votroubek, Phys. Rev. Lett. **94**, 185001 (2005).
[20] A. L. Hoffman, H. Y. Guo, K. E. Miller, and R. D. Milroy, Nucl. Fusion **45**, 176 (2005).
[21] H. Y. Guo, A. L. Hoffman, and L. C. Steinhauer, Phys. Plasmas **12**, 062507 (2005).
[22] S. Okada, K. Kitano, H. Sumikura, T. Higashikozono, M. Inomoto, S. Yoshimura, and M. Ohta, Nucl. Fusion **45**, 1094 (2005).
[23] A. L. Hoffman, H. Y. Guo, K. E. Miller, and R. D. Milroy, Phys. Plasmas **13**, 012507 (2006).
[24] H. Y. Guo, A. L. Hoffman, L. C. Steinhauer, K. E. Miller, and R. D. Milroy, Phys. Rev. Lett. **9**, 235002 (2006).
[25] A. S. Landsman, S. A. Cohen, and A. H. Glasser, Phys. Rev. Lett. **96**, 015002 (2006).
[26] S. A. Cohen, B. Berlinger, C. Brunkhorst, A. Brooks, N. Ferraro, D. P. Lundberg, A. Roach, and A. H. Glasser, Phys. Rev. Lett. **98**, 145002 (2007).
[27] Y. Ono, A. Morita, T. Itajaki, and M. Katsurai, Plasma Physics and Controlled Fusion Research, IAEA-CN-56/C-4-4, IAEA, Vienna 1.
[28] E. Kawamori, T. Sumikawa, H. Imanaka, R. Imazawa, K. Yamashita, T. Hayamizu, K. Umeda, and Y. Ono, Paper ex-p7-13, IAEA Fusion Energy Conference, Chengdu, China (2006).
[29] S. P. Gerhardt, E. V. Belova, M. Yamada, H. Ji, M. Inomoto, Y. Ren, and B. McGeehan, Phys. Rev. Lett. **99**, 245003 (2007).
[30] I. B. Bernstein, E. A. Freiman, M. D. Kruskal, and R. M. Kulsrud, Proc. R. Soc. London, Ser. A **244**, 17 (1958).
[31] M. N. Rosenbluth and M. N. Bussac, Nucl. Fusion **19**, 489 (1979).
[32] J. H. Hammer, Nucl. Fusion **21**, 488 (1981).
[33] J. R. Cary, Phys. Fluids **24**, 2239 (1981).
[34] R. A. Clemente and J. L. Milovich, Phys. Fluids **26**, 1874 (1983).
[35] R. Horiuchi, and T. Sato, Phys. Fluids B **1**, 581 (1989).
[36] A. Ishida, N. Shibata, and L. C. Steinhauer, Phys. Plasmas **1**, 4022 (1994).
[37] R. D. Milroy, D. C. Barnes, R. C. Bishop, and R. B. Webster, Phys. Fluids B **1**, 1225 (1989).
[38] E. Belova, S. C. Jardin, H. Ji, M. Yamada, and R. Kulsrud, Phys. Plasmas **7**, 4996 (2000).
[39] E. Belova, S. C. Jardin, H. Ji, M. Yamada, and R. Kulsrud, Phys. Plasmas **8**, 1267 (2001).
[40] N. Iwasawa, A. Ishida, and L. C. Steinhauer, Phys. Plasmas **8**, 1240 (2001).
[41] E. Belova, R. C. Davidson, H. Ji, and M. Yamada, Phys. Plasmas **10**, 2361 (2003).
[42] E. Belova, R. C. Davidson, H. Ji, and M. Yamada, Phys. Plasmas **11**, 2523 (2004).
[43] E. Belova, R. C. Davidson, H. Ji, and M. Yamada, Phys. Plasmas **13**, 056115 (2006).
[44] W. T. Armstrong, R. K. Linford, J. Lipson, D. A. Platts, and E. G. Sherwood, Phys. Fluids **24**, 2068 (1981).
[45] M. N. Rosenbluth, N. A. Krall, and N. Rostoker, Nucl. Fusion Suppl. **1**, 143 (1962).
[46] S. P. Gerhardt, E. Belova, M. Inomoto, M. Yamada, H. Ji, Y. Ren, and A. Kuritsyn, Phys. Plasmas **13**, 112508 (2006).
[47] M. Yamada, H. Ji, S. P. Gerhardt, E. V. Belova, R. C. Davidson, and D. R. Mikkelsen, J. Plasma Fusion Res. **2**, 004 (2007).
[48] M. Yamada, H. Ji, S. Hsu, T. Carter, R. Kulsrud, N. Bretz, F. Jobes, Y. Ono, and R. Perkins, Phys. Plasmas **4**, 1936 (1997).
[49] D. D. Ryutov, J. Kesner, and M. E. Mauel, Phys. Plasmas **11**, 2318 (2004).
[50] H. Y. Guo, A. L. Hoffman, and R. D. Milroy, Phys. Plasmas **14**, 112502 (2007).
[51] D. C. Barnes and R. D. Milroy, Phys. Fluids B **3**, 2609 (1991).
[52] T. Asai, Y. Suzuki, T. Yoneda, F. Kodera, M. Okuba, S. Okada, and S. Goto, Phys. Plasmas **7**, 2294 (2000).
[53] S. Okada, T. Asai, K. Kodera, K. Kitano, Y. Suzuki, K. Yamanaka, T. Kanki, M. Inomoto, S. Yoshimura, M. Okubo, S. Sugimoto, S. Ohi, and S. Goto, Nucl. Fusion **41**, 625 (2001).
[54] T. Asai, M. Inomoto, N. Iwsawa, S. Okada, and S. Goto, Phys. Plasmas **10**, 3608 (2003).
[55] A. B. Hassam, R. M. Kulsrud, R. J. Goldston, H. Ji, and M. Yamada, Phys. Rev. Lett. **83**, 2969 (1999).
[56] H. L. Berk, H. Momota, and T. Tajima, Phys. Fluids **30**, 3548 (1987).
[57] S. P. Auerbach and W. C. Condit, Nucl. Fusion **21**, 927 (1981).
[58] Y. Ono, T. Matsuyama, K. Umeda, and E. Kawamori, Nucl. Fusion **43**, 649 (2003).
[59] C. D. Cothran, A. Falk, A. Fefferman, M. Landreman, M. R. Brown, and M. J. Schaffer, Phys. Plasmas **10**, 1748 (2003).
[60] A. M. M. Todd, M. S. Chance, J. M. Greene, R. C. Grimm, J. L. Johnson, and J. Manickam, Phys. Rev. Lett. **38**, 826 (1977).
[61] L. Sparks, J. M. Finn, and R. N. Sudan, Phys. Fluids **23**, 611 (1980).
[62] M. Tuszewski, D. C. Barnes, R. E. Chrien, J. W. Cobb, D. J. Rej, R. E. Siemon, D. P. Taggart, and B. L. Wright, Phys. Rev. Lett. **66**, 711 (1991).
[63] M. Tuszewski, D. P. Taggart, R. E. Chrien, D. J. Rej, R. E. Siemon, and B. L. Wright, Phys. Fluids B **3**, 2856 (1991).
[64] J. T. Slough, A. L. Hoffman, R. D. Milroy, E. A. Crawford, M. Cecik, R. Maqueda, G. A. Wurden, Y. Itoh, and A. Shiokawa, Phys. Rev. Lett. **69**, 2212 (1992).
[65] J. T. Slough and A. L. Hoffman, Phys. Fluids B **5**, 4366 (1993).
[66] A. Ishida, H. Momota, and L. C. Steinhauer, Phys. Fluids **31**, 3024 (1988).
[67] S. Ohi, T. Minato, Y. Kawakami, M. Tanjyo, S. Okada, T. Ito, M. Kako, S. Goto, T. Ishimura, and H. Ito, Phys. Rev. Lett. **51**, 1042 (1983).
[68] A. L. Hoffman, J. T. Slough, and D. G. Harding, Phys. Fluids **26**, 1626 (1983).
[69] M. Yamada, H. Ji, T. A. Carter, S. C. Hsu, R. M. Kulsrud, N. L. Bretz, F. C. Jobes, Y. Ono, M. Katsurai, T.-H. Watanabe, T. Sato, and T. Hayashi, 16th IAEA Fusion Energy Conference, Montreal, Canada (International Atomic Energy Agency, Vienna, 1996), Paper IAEA-CN-64/CP-19.
[70] M. Inomoto, S. P. Gerhardt, M. Yamada, H. Ji, E. Belova, A. Kuritsyn, and Y. Ren, Phys. Rev. Lett. **97**, 135002 (2006).
[71] M. Yamada, H. P. Furth, W. Hsu, A. Janos, S. Jardin, S. Okbayashi, J. Sinnis, T. H. Stix, and K. Yamazaki, Phys. Rev. Lett. **46**, 188 (1981).
[72] K. Miyamoto, *Plasma Physics for Nuclear Fusion* (MIT Press, Cambridge, MA, 1989).
[73] F. Trintchouk, M. Yamada, H. Ji, R. M. Kulsrud, and T. A. Carter, Phys. Plasmas **10**, 319 (2003).
[74] A. Kuritsyn, M. Yamada, S. Gerhardt, H. Ji, R. Kulsrud, and Y. Ren, Phys. Plasmas **13**, 055703 (2006).
[75] D. J. Rej, G. A. Barnes, M. H. Baron, R. E. Chrien, S. Okada, R. E. Siemon, D. P. Taggert, M. Tuszewski, R. B. Webster, and B. L. Wright, Phys. Fluids B **2**, 1706 (1990).
[76] E. Chao, "Pure electron plasma dynamics and the effects of collisions with background neutral gas atoms," Ph.D. thesis, Princeton University (1999).
[77] W. Lotz, Report IPP 1/62, "Electron impact cross-sections and ionization rate coefficients for atoms and ions from hydrogen to calcium," Institute for Plasma Physics, Garching (1967).
[78] S. Ejima, R. W. Callis, J. L. Luxon, R. D. Stambaugh, T. S. Taylor, and J. C. Wesley, Nucl. Fusion **22**, 1313 (1982).
[79] W. A. Houlberg, Nucl. Fusion **27**, 1009 (1987).
[80] J. E. Menard, B. P. LeBlanc, S. A. Sabbagh, M. G. Bell, R. E. Bell, E. D. Fredrickson, D. A. Gates, S. C. Jardin, D. W. Johnson, S. M. Kaye, H. W. Kugel, R. Maingi, R. J. Maqueda, D. Mueller, M. Ono, F. Paoletti, S. F. Paul, C. H. Skinner, D. Stutman, and The NSTX Research Team, Nucl. Fusion **41**, 1197 (2001).
[81] Y. Ono, M. Yamada, Y. Akao, T. Tajima, and R. Matsumoto, Phys. Rev. Lett. **76**, 3328 (1996).
[82] H. Ji, M. Yamada, R. Kulsrud, N. Pomphrey, and H. Himura, Phys. Plasmas **5**, 3685 (1998).
[83] J. K. Anderson, C. B. Forest, T. M. Biewer, J. S. Sarff, and J. C. Wright, Nucl. Fusion **44**, 162 (2004).
[84] J. Wesson, *Tokamaks* (Clarendon Press, Oxford, 1987).

Downloaded 21 Jul 2008 to 198.35.13.204. Redistribution subject to AIP license or copyright; see http://pop.aip.org/pop/copyright.jsp